Journal of Superconductivity and Novel Magnetism (2018) 31:3981–3987
https://doi.org/10.1007/s10948-018-4671-2

ORIGINAL PAPER

Quantification of the Interaction Field in Arrays of Magnetic Nanowires from the Remanence Curves

Elsie Araujo[1] · Juan Manuel Martínez-Huerta[1] · Luc Piraux[2] · Armando Encinas[1]

Received: 31 January 2018 / Accepted: 27 March 2018 / Published online: 5 April 2018

Abstract

A method is presented that allows quantifying the average value of the interaction field in arrays of magnetic nanowires from the field difference between the isothermal remanence (IRM) and the DC demagnetizing (DCD) remanence curves when the normalized magnetization is equal to one third. Arrays of magnetic nanowires of different diameters and packing fractions are used to experimentally test the method. The results have been compared with those obtained using the method based on the difference between the remanence coercivity fields and with a mean-field expression for the interaction field, providing a very good agreement and thus validating the method. Additionally, it is shown that both the position (m_0) and the shift along the magnetization axis of the intersection between the remanence curves with respect to the value of one third ($\delta m = m_0 - 1/3$) provide qualitative information about the interaction field. The former indicates the type of interaction depending if the intersection is above ($m_0 > 1/3$) or below ($m_0 < 1/3$), which corresponds to a ferro or anti-ferro magnetic interaction, respectively. While for the latter, it is shown that the maximum deviation of the Delta-M plot from zero (ΔM_{max}) corresponds to three times the shift ($\Delta M_{max} = 3\delta m$).

Keywords Dipolar interaction · Remanence curves · Delta-M plot · Magnetic nanowires

1 Introduction

Assemblies or arrays made of magnetic nanostructures have been and are currently of great interest due to the variety and complexity of their magnetic properties as well as for their known technological potential [1, 2]. This type of systems, include micro and nanoparticle assemblies [3, 4], granular films [5, 6], composites with magnetic particles dispersed in a non-magnetic matrix [7], multiferroic composites [8], and patterned thin films and multilayers [9], whose applications include magnetic recording materials [9, 10], sensors, programmable magnonic devices [11], microwave devices [12], spin torque resonance [13], nanomedicine [14], and magnetic refrigeration [15].

✉ Armando Encinas
armando.encinas@ipicyt.edu.mx

[1] División de Materiales Avanzados, Instituto Potosino de Investigación Científica y Tecnológica, Caminio a la Presa San José 2055, 78216 San Luis Potosí, San Luis Potosí, Mexico

[2] Institute of Condensed Matter and Nanosciences, Université catholique de Louvain, Place Croix du Sud 1, 1348, Louvain-la-Neuve, Belgium

The response of these materials to an applied external field is known to depend on the magnetic properties of each of the individual particles and also on the interactions between them [16, 17]. Therefore, interaction effects are of key importance for tuning the magnetic properties since they contribute to the total energy of the system and the strength of this contribution with respect to the self energy of the individual constituents can drastically change the magnetic properties [18, 19]. Examples of these effects are the broadening of the intrinsic switching field distribution [20], frustration in nanomagnetic artificial spin ice [21], superferromagnetic collective behavior [22, 23], and heating efficiency in magnetic cancer hyperthermia [24–28], among others.

Measurement of the interaction field has remained a difficult problem. The first methods used to gain qualitative information about the interaction field were the Henkel and Delta-M plots [29, 30]. More recently, other methods have provided different approaches that allow quantifying the interaction field, among these the Delta-H method [31, 32], FORC diagrams [33–37], the minor loop shift [38], and ferromagnetic resonance in both saturated [39] as well as non-saturated states [40] and from the energy barrier shift [41]. The major difficulty regarding the measurement of the interaction field is that it cannot be directly measured

from magnetization curves. In particular, in order to quantify the interaction field using the remanence curves and Wohlfarth's relation, it is necessary to find either graphical representations or coordinates from which the difference between the interacting and non-interacting cases can be determined as field differences and then establishing relations between these differences and the magnitude of the interaction field. Henkel and Delta-M plots, despite their regular use [42–44], can only provide qualitative information about the interaction field since they give a graphical description of the interaction effects as a function of magnetization differences, differences that cannot be easily related to the interaction field. Besides graphical representations, the use of specific coordinates of the remanence curves can also give information about interaction effects. Corradi and Wohlfarth [45] introduced the interaction field factor (IFF) defined as the difference between the fields where the DCD curve is zero (H_d^0) and where the IRM curve is 1/2 ($H_r^{0.5}$) normalized by H_d^0. The use of these fields follows from noting that when there is no interaction, the Wohlfarth relation requires them to be equal, but in the interacting case they are different and the difference can be measured. This quantity is based on a field difference but due to the normalization by H_0, it is dimensionless, so its magnitude and sign only provide qualitative information about the interaction field. A later refinement to this quantity, equivalent to 2 × IFF [46], is also dimensionless and therefore it cannot provide a field value for the interaction field. In this sense, a quantitative determination of the interaction field was reported, which is based on the same field difference, namely $2 \times \text{IFF} \times H_d^0$ [47].

In the present study, it is shown that the field difference between the IRM and DCD remanence curves at a normalized magnetization value of $m = 1/3$ is proportional to the interaction field. The rationale is based on the fact that for a non-interacting assembly, Wohlfarth's relation requires both remanence curves to intersect at $m = 1/3$. However, in the presence of an interaction, the curves intersect at a different magnetization value resulting in a measurable field difference at $m = 1/3$. A simple relation has been obtained between this field difference and the strength of the interaction field.This relation has been tested and validated performing measurements on arrays of magnetic nanowires (NWs) and comparing the results with those obtained using the difference between the remanent coercivity fields [47] as well as with a mean field expression for tall NWs. Finally, it is shown that from the shift of the normalized magnetization where both remanence curves intersect with respect to $m = 1/3$ (δm), it is possible to (a) infer the type of interaction, e.g, the interaction is ferromagnetic if the intersection is above $m = 1/3$ and anti-ferromagnetic if the intersection is below $m = 1/3$, and (b) the maximum amplitude of the Delta-M plot (ΔM_{max}) is shown to be $\Delta M_{max} = 3\delta m$.

2 Experimental

$Ni_{80}Fe_{20}$ and $Co_{45}Fe_{55}$ nanowires have been grown by electrodeposition into the pores of track-etched Polycarbonate (PC) with a 21 μm thickness (from it4ip S. A.) and 90 μm thick Anodized Alumina Oxide (AAO) membranes (from Synkera Technologies) [48]. In these templates, the nanopores are parallel to each other; but in PC membranes, the pores are randomly ordered while in AAO the pores are hexagonally ordered. For both membranes, their porosity P is taken as the NW packing fraction. Prior to the electrodeposition, a Cr/Au layer is evaporated on one side of the membrane to serve as a cathode. Electrodeposition was done at room temperature, using a constant potential measured versus an Ag/AgCl reference electrode and a Pt working electrode. NiFe was grown at $V = -1.0$ V from a 5.56 g/l $FeSO_4$+ 131.42 g/l $NiSO_4$ + 30 g/l H_3BO_3 electrolytic solution. The CoFe samples were grown from a 40 g/l $FeSO_4$+ 80 g/l $CoSO_4$ + 30 g/l H_3BO_3 solution at a potential of $V = -1.0$ V. To assure that all the NWs have a high aspect ratio, their height was kept to approximately 90% of the membrane thickness for PC and above 50% for AAO. The details of the nanowire samples considered in the present study are presented in Table 1.

Room temperature magnetometry measurements were done using an alternating gradient magnetometer with the field applied along the wires axes, and both DCD and IRM remanence curves were normalized to the saturation value of the IRM remanence curve.

3 Results

3.1 Quantification of the Interaction Field

Figure 1(a) shows the IRM and DCD remanence curves, m_r and m_d, respectively along with the major hysteresis loop. The IRM curve, m_r, is measured by applying and removing an increasingly positive field with the sample initially demagnetized, until the highest remanent magnetization is attained. When the field is removed after each field increment, the remanent magnetization is measured along with the final field value of the corresponding increment. The DCD curve, m_d, starts at the highest positive remanence value after applying and removing a large positive magnetic field, and by applying and removing an increasingly negative field, the system is taken to the final state where remanence has its maximum value but in the negative direction.

For a non-interacting particle assembly, m_r and m_d follow the Wohlfarth relation [49],

$$m_d = 1 - 2m_r, \tag{1}$$

Table 1 Material, template, wire diameter (ϕ), and membrane porosity (P) of the nanowire arrays used in this study

	Template	ϕ (nm)	P (%)	$\alpha_{1/3}$ (Oe)	α_0 (Oe)	α_z (Oe)	δm	ΔM_{max}
CoFe	PC	70	0.2	19	20	24	−0.033	−0.098
CoFe	PC	35	5.0	626	662	635	−0.127	−0.376
CoFe	AAO	18	11	1420	1380	1430	−0.234	−0.700
NiFe	PC	50	4.5	210	214	223	−0.143	−0.434
NiFe	AAO	18	7.0	325	344	350	−0.159	−0.480
NiFe	AAO	35	12	641	604	600	−0.214	−0.630

Values of the interaction field coefficient (α) measured from the shift at $m = 1/3$ ($\alpha_{1/3}$), from the remanent coercivity field difference (α_0) and the theoretical value (α_z). IRM and DCD intersection shift with respect to $m = 1/3$, δm, and the maximum deviation of the Delta-M curve with respect to zero ΔM_{max}

so for a given field value, H_i on m_r and $-H_i$ on m_d, both curves should have magnetization values so that $m_d - [1 - 2m_r] = 0$ [30]. To compare them graphically, m_d is often plotted as the field-reflected $m_d(-H)$ so it runs over positive field values, as shown in Fig. 1(b). If there is no interaction, $m_d(-H)$ and the curve $1 - 2m_r$ are identical. This is shown in Fig. 1(b) or the CoFe NWs with 70 nm diameter and $P = 0.2\%$ which has a very small interaction field, and as seen from the figure, both curves are almost identical.

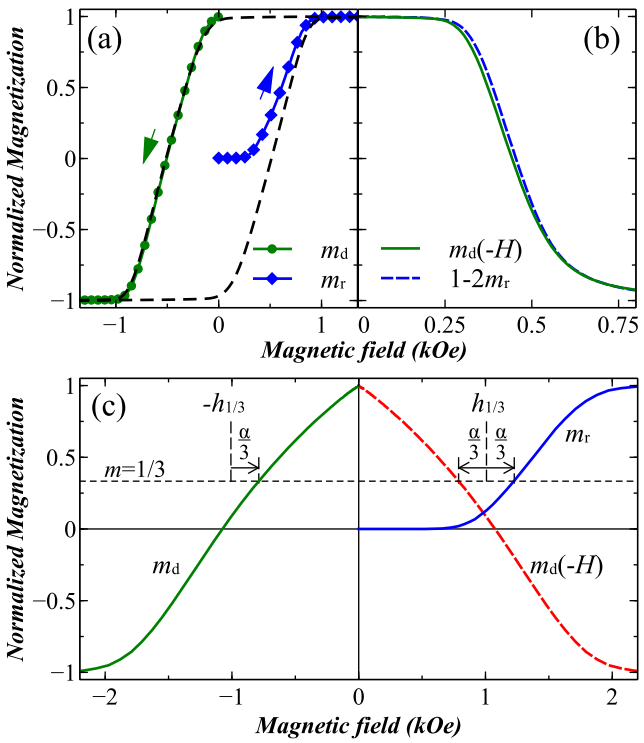

Fig. 1 **a** IRM and DCD remanence curves, m_r and m_d, respectively along with the major hysteresis loop for NiFe NWs with 50 nm diameter and $P = 4.5\%$. **b** Comparison between the field reflected DCD curve $m_d(-H)$ and the curve $1 - 2m_r$, for the CoFe NWs with 70 nm diameter and $P = 0.2\%$, and **c** IRM remanence curve, m_r, the DCD curve m_d, and the field reflected DCD $m_d(-H)$ corresponding to the NiFe NWs with 30 nm diameter and $P = 12\%$

As observed in Fig. 1(c), the curves $m_d(-H)$ and m_r intersect each other. If there is no interaction, it follows from (1) that these curves intersect at $m = 1/3$ and $H = h_{1/3}$. Several reports have characterized assemblies of particles with vanishing interaction, where it can be verified that the remanence curves intersect at $m = 1/3$ [23, 42, 50, 51]. Since $m_d(-H)$ is the field-reflected m_d curve, then the field value where $m_d = 1/3$ is $H = -h_{1/3}$.

When the particles interact, both remanence curves are sheared by the interaction field; (1) is no longer valid and as seen in Fig. 1c, the curves intersect at a different value of m. To account for this shearing, the usual mean-field approach used for remanence curves [47] and FORC diagrams [33–37] is employed. Namely, the magnetization-dependent interaction field is written as $H = \alpha m$. Here, α is the interaction field at saturation where $\alpha > 0$ implies an antiferromagnetic interaction and for $\alpha < 0$ the interaction is ferromagnetic. Then the total field (H_T), also known as operative field [35], experienced by a given particle in the assembly, corresponds to the sum of the applied field (H_A) and the interaction field, which is,

$$H_T = H_A + \alpha m \tag{2}$$

So each point in the $M(H)$ curve is shifted (sheared) as a result of the sum of the applied and interaction fields. Regarding the shearing on the remanence curves, consider the case for an anti-ferromagnetic interaction ($\alpha > 0$) as is the case of NW arrays. For the IRM curve, $m_r > 0$ and all the points in the curve are shifted to higher fields, as expected from (2). For $m = 1/3$, the field will be shifted by $\alpha/3$ with respect to the field value expected when there is no interaction, previously defined as $h_{1/3}$, as indicated in Fig. 1(c). Then the field value where $m_r = 1/3$ is $H = h_{1/3} + \alpha/3$.

For $m_d = 1/3$, the shift is the same, $\alpha/3$, and since $\alpha > 0$ the shift is also done toward more positive fields. So, as seen in Fig. 1(c), the field value where $m_d = 1/3$ is $H = -h_{1/3} + \alpha/3$. For the field-reflected DCD curve, $m_d(-H)$, the fields change sign and the shearing is done in the opposite sense, so $H = h_{1/3} - \alpha/3$.

It follows that when $m = 1/3$, the m_r curve is shifted by $H = \alpha/3$ toward higher fields, while $m_d(-H)$ is shifted by the same quantity but in opposite direction, toward lower fields, as indicated in Fig. 1(c); so the field difference between them is $\Delta H_{1/3} = 2(\alpha/3)$, and therefore the interaction field can be written as,

$$\alpha = \frac{3}{2}\Delta H_{1/3} \tag{3}$$

To test this expression, the field difference $\Delta H_{1/3}$ has been determined on all the samples for which the interaction field coefficient has been obtained. Figure 2 shows the IRM and the field-reflected DCD remanence curve for the three CoFe samples in order of increasing packing fraction: (a) 70 nm diameter and $P = 0.2\%$, (b) 35 nm diameter and $P = 5\%$, and (c) 18 nm diameter and $P = 12\%$. As seen in the figure, the field difference $\Delta H_{1/3}$ increases with the packing fraction and thus with the strength of the interaction field. Notice that for the case of a very weak interaction, Fig. 2(a), the intersection is very close to $m = 1/3$. In order to compare the results obtained with this method, the interaction field coefficient has also been measured using the difference of the remanent coercivity fields of the IRM and DCD curves using [47],

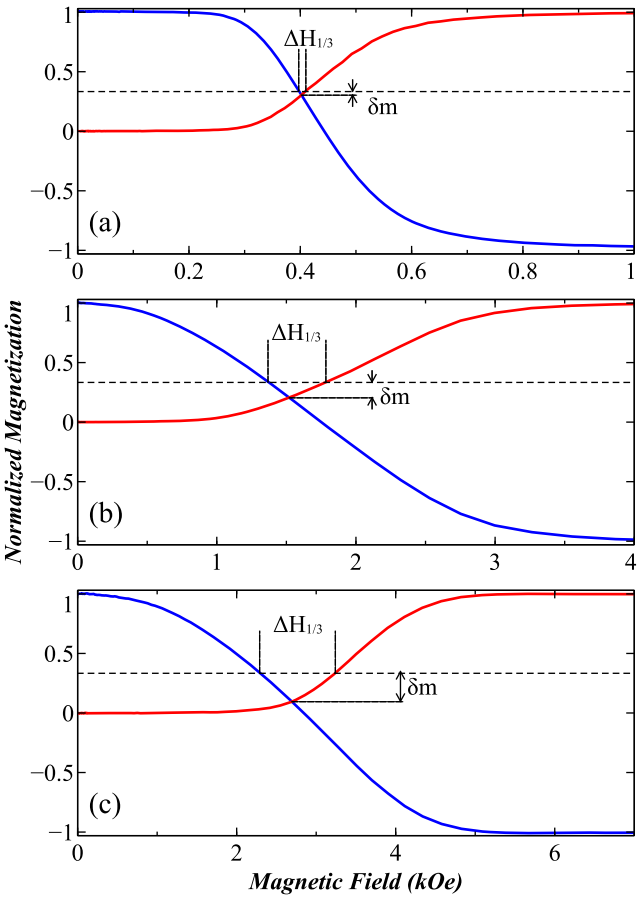

Fig. 2 IRM remanence curve, m_r, and the field-reflected DCD remanence curve $m_d(-H)$ measured on CoFe NWs with **a** 70 nm diameter and $P = 0.3\%$ where $\Delta H_{1/3} = 10.8$ Oe, **b** 35 nm diameter and $P = 5\%$ with $\Delta H_{1/3} = 411$ Oe, and **c** 18 nm diameter and $P = 12\%$ and $\Delta H_{1/3} = 944$ Oe. In all cases, the horizontal dashed line corresponds to $m = 1/3$ and the distance between $m = 1/3$ and where the remanence curves intersect is indicated as δm

$$\alpha_0 = 2(H_r^{0.5} - H_d^0) \tag{4}$$

where $H_r^{0.5}$ is the field where $m_r = 1/2$ and H_d^0 is the field where $m_d(-H) = 0$. The results are listed as α_0 in Table 1, from where it can be seen that both methods provide essentially the same results. This also shows that both methods provide a measurement of the interaction field directly from the IRM and DCD curves, which allows to verify if the measurements are correct.

Moreover, the interaction field coefficient at saturation (α) for arrays of high aspect ratio NWs has been shown to correspond to the component along the wire axis of the magnetization-dependent interaction field, which is given by [52],

$$\alpha_z = 2\pi M_s P \tag{5}$$

where M_s is the saturation magnetization of the material. These values have been calculated for each sample using $M_s = 1900$ emu/cm^3 for $Co_{45}Fe_{55}$ and 800 emu/cm^3 for $Ni_{80}Fe_{20}$ NWs, and the results are shown in Table 1 as α_z. Comparing these results, a very good agreement is found between the experimental values and those derived from (5), which further validates (3).

3.2 Qualitative Features of the Intersection of the Remanence Curves

In this section, it is shown that the coordinate where the remanence curves intersect provides qualitative information about the interaction field.

Consider the intersection of the m_r and $m_d(-H)$ remanence curves, hereafter (h_0, m_0). For any value of the interaction different than zero, both curves are sheared so that $m_0 \neq 1/3$ and the difference between these values is,

$$\delta m = m_0 - \frac{1}{3} \tag{6}$$

If there is no interaction, there is no shearing of the remanence curves and $m_0 = 1/3$ and $\delta m = 0$. Then, if the interaction is antiferromagnetic, every point in m_r ($m_d(-H)$) is shifted to higher (lower) fields, and their intersection occurs at $m_0 < 1/3$ and $\delta m < 0$. Inversely, if the interaction is ferromagnetic, every point in m_r ($m_d(-H)$) is shifted to lower (higher) fields, and the curves intersect at $m_0 > 1/3$ and and $\delta m > 0$. Therefore, the type

of interaction can be determined from the value of m_0 or the sign of δm, and since the amount of shearing is proportional to the strength of the interaction field, the value of $|\delta m|$ increases with the interaction field. This is seen in Fig. 2 for the CoFe NWs with packing fractions of (a) 0.3%, (b) 5%, and (c) 12%. In all cases, $m_0 < 1/3$ and $\delta m < 0$ consistent with an antiferromagnetic interaction. The values of δm for all the sample are listed in Table 1, where it is seen that it increases with the interaction field. The fact that the sign and magnitude of δm are qualitatively related to the nature and strength of the interaction field suggests that this quantity is related to the Delta-M plot. Indeed, from (1), Delta-M is $\Delta M = m_d - [1 - 2m_r]$ [30], then for $m_d = m_r = m_0$ and using (6), it follows that $\Delta M = 3\delta m$. This suggests that the maximal deviation of the Delta-M plot with respect to zero is $3\delta m$. To confirm this, Fig. 3(a) shows the Delta-M plots of the CoFe NWs with 70 nm diameter and $P = 0.3\%$, 35 nm diameter and $P = 5\%$, and 18 nm diameter and $P = 12\%$ while Fig. 3(b) presents the same Delta-M plots normalized by the corresponding value of $3\delta m$. As seen from the figure, normalizing each Delta-M plot by their corresponding value of $3\delta m$, their amplitudes become equal. So that the maximum value of the Delta-M plot is such that $\Delta M_{max} = 3\delta m$. For reference, the values of δm and ΔM_{max} are shown in Table 1.

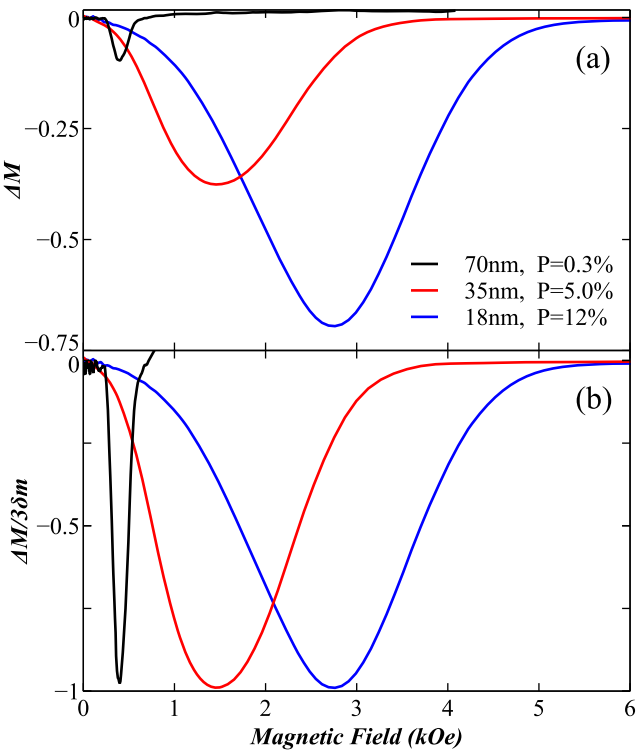

Fig. 3 **a** Delta-M plots of the CoFe NWs with 70 nm diameter and $P = 0.3\%$, 35 nm diameter and $P = 5\%$ and 18 nm diameter and $P = 12\%$ and **b** the same Delta-M plots normalized by the corresponding value of $3\delta m$

4 Discussion

The results show that the value of the interaction field in NW arrays can be quantified using the remanence curves and (3). The value delivered by this method corresponds to the average value of the interaction field coefficient at saturation (α), which is the same quantity obtained by other methods that provide a single valued measurement of the interaction field, such as FORC diagrams [33–37] or other methods based on the remanence curves [47]. The method has the advantage of using well-established protocols, the remanence curves, which provide an easy and rapid approach to quantify the interaction field. Moreover, as shown above, the results can be further verified experimentally using (4). Regarding its applicability and limitations, it is important to underline that the analysis leading to (3) is solely based on a condition imposed by the Wohlfarth relation on the IRM and DCD curves for non-interacting systems. Therefore, it expected to apply to other particle assemblies provided that certain conditions are met. In particular, it must be considered that the Wohlfarth relation is limited to assemblies of either ordered or disordered uniaxial single-domain particles [49]. Another restriction on the use of methods based on the Wohlfarth relation is that they are limited to particle assemblies where no cooperative effects take place, so it is reasonable to consider that the effect of the interaction field can be accurately taken into account as an additive field as in (2) [53]. These conditions imply that the method applies to particle assemblies where each particle has a square hysteresis loop, or approximates an ideal hysteron, capable of switching irreversibly without altering the magnetic state of other particles. For NWs, these considerations are valid for low diameters (<100 nm) which behave as macrospins [36] and packing fractions bellow 15%.

Finally, the method to quantify the interaction field using (3) is complementary to other magnetic analysis tools such as FORC diagrams. These diagrams provide richer information about particle assemblies and allow analyzing more complex systems. However, they are based on a different measuring approach. Specifically, remanence curves only contain information about irreversible switching processes, while FORC diagrams are based on recoil curves which contain information about both reversible and irreversible switching processes. Therefore, an analysis combining both methods could provide more insight to the system under consideration than using only one of these methods alone.

Regarding the qualitative features of the intersection between the IRM and DCD remanence curves and δm, it is important to note that these remain entirely qualitative. However, they have the advantage of avoiding the actual construction of the Delta-M plots, since the direct

analysis of the IRM and DCD plots and the position of the intersection can show the presence and nature of the interaction.

5 Conclusion

In conclusion, we have shown that the value of the interaction field coefficient in NW arrays can be obtained directly from the normalized IRM and DCD remanence curves using the field difference between these curves when the magnetization is equal to one third. Moreover, the intersection between the remanence curves in interacting systems provides the same qualitative information about the interaction as the Delta-M plots while it is also related to the position and value of the point where the Delta-M plot is maximum. The method is relevant as it provides a very simple way to quantify the average value of the interaction field through the direct use of standard measurements such as the IRM and DCD remanence curves.

Acknowledgements The authors thank E. Ferain of it4ip S. A. for providing the PC membranes. E. Araujo thanks Fondo CONACYT-Secretaría de Energía - Sustentabilidad Energética.

Funding Information This study received financial support from CONACYT Ciencia Básica grant 286626 and CONACYT-SENER I0027-2015-01-232611, and Fédération Wallonie-Bruxelles (ARC 13/18-052, Supracryst) and Fonds de la Recherche Scientifique-FNRS under grant no. T.0006.16.

References

1. Sander, D., et al.: The 2017 magnetism roadmap. J. Phys. D: Appl. Phys. **50**, 363001 (2017)
2. Fernández-Pacheco, A., Streubel, R., Fruchart, O., Hertel, R., Fischer, P., Cowburn, R.P.: Three-dimensional nanomagnetism. Nat. Commun. **8**, 15756 (2017)
3. Shi, W., Liang, R., Xu, S., Wang, Y., Luo, C., Darwish, M., Smoukov, S.K.: Layer-by-layer self-assembly: toward magnetic films with tunable anisotropy. J. Phys. Chem. C **119**(23), 13215 (2015)
4. Klughertz, G., Manfredi, G., Hervieux, P.A., Pichon, B.P., Begin-Colin, S.: Effect of disorder and dipolar interactions in two-dimensional assemblies of iron-oxide magnetic nanoparticles. J. Phys. Chem. C **120**(13), 7381 (2016)
5. Okamoto, S., Kikuchi, N., Hotta, A., Furuta, M., Kitakami, O., Shimatsu, T.: Microwave assistance effect on magnetization switching in Co-Cr-Pt granular film. Appl. Phys. Lett. **103**(20), 202405 (2013)
6. Kumar, D., Chaudhary, S., Pandya, D.K.: Evolution of particle size and interparticle magnetic interactions with thickness in co-sputtered $Cu_{79}Co_{21}$ nanogranular thin films. J. Appl. Phys. **114**(2), 023908 (2013)
7. Thevenot, J., Oliveira, H., Sandre, O., Lecommandoux, S.: Magnetic responsive polymer composite materials. Chem. Soc. Rev. **42**, 7099 (2013)
8. Ojha, S., Nunes, W.C., Aimon, N.M., Ross, C.A.: Magnetostatic interactions in self-assembled $Co_xNi_{1-x}Fe_2O_4/BiFeO_3$ multiferroic nanocomposites. ACS Nano **10**(8), 7657 (2016). PMID: 27434047
9. Albrecht, T.R., et al.: Bit-patterned magnetic recording: theory, media fabrication, and recording performance. IEEE Trans. Magn. **51**, 1 (2015)
10. Lau, J.W., Shaw, J.M.: Magnetic nanostructures for advanced technologies: fabrication, metrology and challenges. J. Phys. D: Appl. Phys. **44**(30), 303001 (2011)
11. Krawczyk, M., Grundler, D.: Review and prospects of magnonic crystals and devices with reprogrammable band structure. J. Phys. Condens. Matter **26**(12), 123202 (2014)
12. Carignan, L.P., Yelon, A., Menard, D., Caloz, C.: Ferromagnetic nanowire metamaterials: theory and applications. IEEE Trans. Microwave Theory Tech. **59**(10), 2568 (2011)
13. Schreier, M., Chiba, T., Niedermayr, A., Lotze, J., Huebl, H., Geprägs, S., Takahashi, S., Bauer, G.E.W., Gross, R., Goennenwein, S.T.B.: Current-induced spin torque resonance of a magnetic insulator. Phys. Rev. B **92**, 144411 (2015)
14. Long, N.V., Yang, Y., Teranishi, T., Thi, C.M., Cao, Y., Nogami, M.: Biomedical applications of advanced multifunctional magnetic nanoparticles. J. Nanosci. Nanotechnol. **15**(12), 10091 (2015)
15. Bjørk, R., Bahl, C.R.H.: Demagnetization factor for a powder of randomly packed spherical particles. Appl. Phys. Lett. **103**(10), 102403 (2013)
16. Majetich, S.A., Sachan, M.: Magnetostatic interactions in magnetic nanoparticle assemblies: energy, time and length scales. J. Phys. D: Appl. Phys. **39**(21), R407 (2006)
17. Pardavi-Horvath, M.: Interaction effects in magnetic nanostructures. Phys. Status Solidi A **211**(5), 1030 (2014)
18. Stamps, R.L., et al.: The 2014 magnetism roadmap. J. Phys. D: Appl. Phys. **47**, 333001 (2014)
19. Aslibeiki, B., Kameli, P., Salamati, H.: The effect of dipole-dipole interactions on coercivity, anisotropy constant, and blocking temperature of $MnFe_2O_4$ nanoparticles. J. Appl. Phys. **119**(6), 063901 (2016)
20. Pfau, B., Günther, C.M., Guehrs, E., Hauet, T., Hennen, T., Eisebitt, S., Hellwig, O.: Influence of stray fields on the switching-field distribution for bit-patterned media based on pre-patterned substrates. Appl. Phys. Lett. **105**(13), 132407 (2014)
21. Nisoli, C., Moessner, R., Schiffer, P.: Artificial spin ice: designing and imaging magnetic frustration. Rev. Mod. Phys. **85**, 1473 (2013)
22. Bedanta, S., Kleemann, W.: Supermagnetism. J. Phys. D: Appl. Phys. **42**(1), 013001 (2009)
23. Hillion, A., Tamion, A., Tournus, F., Albin, C., Dupuis, V.: From vanishing interaction to superferromagnetic dimerization: experimental determination of interaction lengths for embedded Co clusters. Phys. Rev. B **95**, 134446 (2017)
24. Landi, G.T.: Role of dipolar interaction in magnetic hyperthermia. Phys. Rev. B **89**, 014403 (2014)
25. Salas, G., Camarero, J., Cabrera, D., Takacs, H., Varela, M., Ludwig, R., Dähring, H., Hilger, I., Miranda, R., Morales, M.d.P., Teran, F.J.: Modulation of magnetic heating via dipolar magnetic interactions in monodisperse and crystalline iron oxide nanoparticles. J. Phys. Chem. C **118**(34), 19985 (2014)
26. Ruta, S., Chantrell, R., Hovorka, O.: Unified model of hyperthermia via hysteresis heating in systems of interacting magnetic nanoparticles. Sci. Rep. **5**, 9090 EP (2015)
27. Coral, D.F., Mendoza Zélis, P., Marciello, M., Morales, M.d.P., Craievich, A., Sánchez, F.H., Fernández van Raap, M.B.: Effect of nanoclustering and dipolar interactions in heat generation for magnetic hyperthermia. Langmuir **32**(5), 1201 (2016)
28. Orozco-Henao, J.M., Coral, D.F., Muraca, D., Moscoso-Londoño, O., Mendoza Zélis, P., Fernandez van Raap, M.B., Sharma, S.K.,

Pirota, K.R., Knobel, M.: Effects of nanostructure and dipolar interactions on magnetohyperthermia in iron oxide nanoparticles. J. Phys. Chem. C **120**(23), 12796 (2016)
29. Henkel, O.: Remanenzverhalten und wechselwirkungen in hartmagnetischen teilchenkollektiven. Phys. Status Solidi B **7**(3), 919 (1964)
30. Kelly, P.E., O'Grady, K., Mayo, P.I., Chantrell, R.W.: Switching mechanisms in cobalt-phosphorus thin films. IEEE Trans. Magn. **25**(5), 3881 (1989)
31. Veitch, R.J.: Anhysteretic susceptibility and static magnetic properties of interacting small particles. IEEE Trans. Magn. **26**(5), 1876 (1990)
32. Harrell, J.W., Richards, D., Parker, M.R.: Delta-h plot evaluation of remanence behavior in barium ferrite tapes and disks. J. Appl. Phys. **73**(10), 6722 (1993)
33. Béron, F., Clime, L., Ciureanu, M., Ménard, D., Cochrane, R.W., Yelon, A.: Magnetostatic interactions and coercivities of ferromagnetic soft nanowires in uniform length arrays. J. Nanosci. Nanotechnol. **8**(6), 2944 (2008)
34. Béron, F., Ménard, D., Yelon, A.: First-order reversal curve diagrams of magnetic entities with mean interaction field: a physical analysis perspective. J. Appl. Phys. **103**(7), 07D908 (2008)
35. Stancu, A., Pike, C., Stoleriu, L., Postolache, P., Cimpoesu, D.: Micromagnetic and preisach analysis of the first order reversal curves (forc) diagram. J. Appl. Phys. **93**(10), 6620 (2003)
36. Dobrotă, C.I., Stancu, A.: What does a first-order reversal curve diagram really mean? a study case: array of ferromagnetic nanowires. J. Appl. Phys. **113**(4), 043928 (2013)
37. Gilbert, D.A., Zimanyi, G.T., Dumas, R.K., Winklhofer, M., Gomez, A., Eibagi, N., Vicent, J.L., Liu, K.: Quantitative decoding of interactions in tunable nanomagnet arrays using first order reversal curves. Sci. Rep. **4**, 4204 EP (2014)
38. Wang, T., Wang, Y., Fu, Y., Hasegawa, T., Oshima, H., Itoh, K., Nishio, K., Masuda, H., Li, F.S., Saito, H., Ishio, S.: Magnetic behavior in an ordered Co nanorod array. Nanotechnology **19**(45), 455703 (2008)
39. Encinas-Oropesa, A., Demand, M., Piraux, L., Huynen, I., Ebels, U.: Dipolar interactions in arrays of nickel nanowires studied by ferromagnetic resonance. Phys. Rev. B **63**, 104415 (2001)
40. De La Torre Medina, J., Piraux, L., Olais Govea, J.M., Encinas, A.: Double ferromagnetic resonance and configuration-dependent dipolar coupling in unsaturated arrays of bistable magnetic nanowires. Phys. Rev. B **81**, 144411 (2010)
41. Moya, C., Iglesias, Ó., Batlle, X., Labarta, A.: Quantification of dipolar interactions in $Fe_{3-x}O_4$ nanoparticles. J. Phys. Chem. C **119**(42), 24142 (2015)
42. Dupuis, V., Khadra, G., Hillion, A., Tamion, A., Tuaillon-Combes, J., Bardotti, L., Tournus, F.: Intrinsic magnetic properties of bimetallic nanoparticles elaborated by cluster beam deposition. Phys. Chem. Chem. Phys. **17**, 27996 (2015)
43. Blanco-Andujar, C., Ortega, D., Southern, P., Pankhurst, Q.A., Thanh, N.T.K.: High performance multi-core iron oxide nanoparticles for magnetic hyperthermia: microwave synthesis, and the role of core-to-core interactions. Nanoscale **7**, 1768 (2015)
44. Panagiotopoulos, I., Fang, W., Aït-Atmane, K., Piquemal, J.Y., Viau, G., Dalmas, F., Boué, F., Ott, F.: Low dipolar interactions in dense aggregates of aligned magnetic nanowires. J. Appl. Phys. **114**(23), 233909 (2013)
45. Corradi, A.R., Wohlfarth, E.P.: Influence of densification on the remanence, the coercivities and the interaction field of elongated γ Fe_2O_3 powders. IEEE Trans. Magn. **14**, 861 (1978)
46. Álvarez, N., Leva, E., Valente, R., Mansilla, M., Gómez, J., Milano, J., Butera, A.: Correlation between magnetic interactions and domain structure in A1 FePt ferromagnetic thin films. J. Appl. Phys. **115**, 083907 (2014)
47. Martínez-Huerta, J.M., Medina, J.D.L.T., Piraux, L., Encinas, A.: Self consistent measurement and removal of the dipolar interaction field in magnetic particle assemblies and the determination of their intrinsic switching field distribution. J. Appl. Phys. **111**(8), 083914 (2012)
48. Piraux, L., Encinas, A., Vila, L., Mátéfi-Tempfli, S., Mátéfi-Tempfli, M., Darques, M., Elhoussine, F., Michotte, S.: Magnetic and superconducting nanowires. J. Nanosci. Nanotechnol. **5**(3), 372 (2005)
49. Wohlfarth, E.P.: Relations between different modes of acquisition of the remanent magnetization of ferromagnetic particles. J. Appl. Phys. **29**(3), 595 (1958)
50. Tournus, F., Tamion, A., Hillion, A., Dupuis, V.: Anisotropy evolution of nanoparticles under annealing: benefits of isothermal remanent magnetization simulation. J. Magn. Magn. Mater. **419**, 1 (2016)
51. Peddis, D., Cannas, C., Piccaluga, G., Agostinelli, E., Fiorani, D.: Spin-glass-like freezing and enhanced magnetization in ultra-small $CoFe_2O_4$ nanoparticles. Nanotechnology **21**, 125705 (2010)
52. Martínez-Huerta, J.M., Medina, J.D.L.T., Piraux, L., Encinas, A.: Configuration dependent demagnetizing field in assemblies of interacting magnetic particles. J. Phys. Condens. Matter **25**(22), 226003 (2013)
53. Skomski, R.: Nanomagnetics. J. Phys. Condens. Matter **15**(20), R841 (2003)